Proc. Lunar Sci. Conf. 7th (1976), p. 1345–1363.
Printed in the United States of America

The phase relations, textures, and mineral chemistries of high-titanium mare basalts as a function of oxygen fugacity and cooling rate

THOMAS M. USSELMAN*

The Lunar Science Institute, 3303 NASA Road 1, Houston, Texas 77058

GARY E. LOFGREN

NASA Johnson Space Center, Houston, Texas 77058

Abstract—The high-titanium mare basalts show a wide diversity of textures and paragenetic sequences. The order of appearance of ilmenite and pyroxene is shown to be very sensitive to oxygen fugacity within the lunar range, using both constant temperature and continuous cooling experiments on 74275. At and slightly below the iron-wüstite buffer, ilmenite crystallizes before pyroxene, while under more reducing conditions, pyroxene precedes ilmenite. The oxygen fugacities estimated using the different paragenetic sequences are commensurate with those estimated from a constructed armalcolite oxygen geobarometer, using the calculated Ti^{3+} contents of the equilibrium armalcolites. The estimated oxygen fugacities for the high-titanium mare basalts suggests that a gaseous buffering species may account for different oxygen fugacities within similar chemical groupings.

The textures of the continuous cooling experiments varied as a complex interplay of oxygen fugacity, cooling rate and history, and nucleation kinetics. The nucleation kinetics of the phases have produced heterogeneous textures in some of the experiments which mimic those observed in 70215. An implication of these continuous cooling experiments is that olivine, spinel, armalcolite, and possibly metallic iron were present in the high-titanium lavas upon eruption.

INTRODUCTION

THE APOLLO 17 HIGH-TITANIUM BASALTS show a wide diversity of textures and petrographically inferred paragenetic sequences. El Goresy *et al.* (1974) have noted that there are two distinct paragenetic sequences involving ilmenite, armalcolite, and pyroxenes; they used these sequences to account for the different armalcolite relationships and suggested that they may be cooling rate dependent. Usselman *et al.* (1975) studied a synthetic high-titanium basalt using both constant temperature and controlled cooling rate experiments and demonstrated that the differences in the ilmenite-pyroxene paragenesis were not cooling rate dependent, but related to the oxygen fugacity (f_{O_2}) at which the rock crystallized.

Controlled cooling experiments on synthetic mare basalt compositions have shown that texture and mineral chemistries can be replicated (Lofgren *et al.*, 1974, 1975; Usselman *et al.*, 1975; Donaldson *et al.*, 1975a). Some doubt always lingers, however, when comparing results on synthetic materials to their natural equivalents. Walker *et al.* (1976a) have completed controlled cooling experiments on

*Present address: Department of Geological Sciences, State University of New York, Buffalo, New York 14226.

12002 and shown direct correspondence between experimentally produced samples and natural equivalents. Walker *et al.*, however, have used somewhat different experimental techniques (cf. Donaldson *et al.*, 1975a).

74275 is a fine-grained high-titanium mare basalt (estimated cooling rate of 5–10°/hr, Usselman *et al.*, 1975). Dispersed throughout are microphenocrysts of olivine, armalcolite, and spinel set in a groundmass containing pyroxene, plagioclase, ilmenite, silica, troilite, and metallic iron. Metallic iron and spinel are often included in the olivine phenocrysts (74275,89). Chemically, compared to the other Apollo 17 basalts, 74275 has the highest Mg/(Mg + Fe) and very high Cr_2O_3 (Rhodes *et al.*, 1976) and hence may be considered "primitive." 74275,109 was chosen for this study as it was a split of a 5 g allocation and the chemistry has been determined (S. R. Taylor, pers. comm.; Rhodes *et al.*, 1976). The phase equilibria of 74275 have been determined by two different techniques giving widely different results (O'Hara and Humphries, 1975; Green *et al.*, 1975). One group has spinel on the liquidus, while the others have olivine on the liquidus. Walker (pers. comm.) also stated that the sample gained substantial amounts of iron using the Fe-capsule technique.

It was the purpose of this project to determine: (1) whether f_{O_2}-controlled, crystallization sequences similar to those observed in the synthetic high-titanium basalt (Usselman *et al.*, 1975) exist for the Apollo 17 high-titanium basalts; (2) what implications these sequences have for the f_{O_2} of crystallization; (3) what effects the f_{O_2} has on the mineralogical trends of these basalts; and (4) whether controlled cooling experiments for synthetic analogs adequately duplicate the crystallization behavior of natural basalts.

EXPERIMENTAL TECHNIQUES

Approximately 2 g of 74275,109 were crushed in an agate ball mill to approximately 20 μm. For the constant temperature experiments, 40 mg pressed pellets were placed on a 0.005″ Pt-wire loop and electrically heated until slight sintering or melting (less than 1%) tacks the pellet to the Pt-wire loop (Donaldson *et al.*, 1975). For the cooling experiments, 80 mg pellets were tacked to a 0.008″ Pt-wire loop. Each charge was suspended in a vertical gas-mixing (CO–CO_2) furnace and the oxygen fugacity was monitored directly with a solid-ceramic, electrolytic cell. The experimental assembly and techniques are described by Williams and Mullins (1976). Oxygen fugacity values are expressed in units of atmospheres throughout the paper.

The dynamic crystallization experiments were done at linear cooling rates. A cooling history not previously reported for lunar samples was used, which closely duplicate the textures in 74275 and overcame the plagioclase nucleation problem. The crystalline starting material was partially melted at 1175°C which produced a charge that comprised ~80% liquid and an unmelted fraction that included spinel, armalcolite, and olivine. The linear cooling histories were initiated from that temperature in order to better simulate the extrusion of a magma containing those crystalline phases.

Quenched runs were mounted in epoxy, sectioned, and polished for optical and electron microprobe analyses. Probe analyses were performed at 0.02 μA and 15 kV and corrected using Bence-Albee (1968). Iron loss and sodium loss at near-liquidus temperatures was substantial (~ 10% and 20%, respectively); the losses were less at lower temperatures. The losses are substantially larger than observed for the quartz-normative and olivine-normative synthetic lunar basalts (Lofgren *et al.*, 1974; Donaldson *et al.*, 1975b) and for a terrestrial oceanic thoeliite (Lofgren and Donaldson, 1975). The differences are not understood and may place limits on the Pt-wire loop technique.

Table 1. Experimental runs on 74275,109. Temperatures and oxygen fugacities are believed to be accurate to ± 3°C and ± 0.05 log units, respectively. All runs started with crushed crystalline material.

Temperature, °C	log f_{O_2}	Time, hours	Phases (+ liquid)
1265	− 11.17	18	—
1265	− 12.20	18	Sp + Fe
1230	− 12.02	19	Sp
1230	− 12.61	34	Sp + Ol(tr) + Fe
1220	− 11.89	24	Sp + Ol(tr)
1195	− 12.17	83	Sp + Ol + Ar(tr)
1190	− 13.12	19	Sp + Ol + Ar + Fe
1185	− 14.03	23	Ol + Ar(tr) + Fe
1178	− 13.23	44	Sp + Ol + Ar + Fe
1170	− 12.39	70	Sp + Ol + Ar
1170	− 13.19	40	Sp + Ol + Ar + Fe
1160	− 12.32	70	Sp + Ol + Ar
1160	− 12.83	70	Sp + Ol + Ar + Fe
1160	− 13.40	41	Sp + Ol + Ar + Fe
1152	− 13.01	52	Sp + Ol + Ar + Il(?) + Fe
1152	− 14.02	44	Ol + Ar + Cp + Pg + Fe
1148*	− 13.22	51	Sp + Ol + Ar + Il + Pl + Fe
1148*	− 14.70	51	Ol + Ar + Cp + Pg + Pl + Fe
1145	− 12.84	48	Ol + Ar(tr) + Cp + Il + Pl
1144	− 13.51	78	Sp + Ol + Ar + Cp + Il + Pl + Fe
1142	− 13.97	48	Sp + Ol + Ar + Cp + Pg + Il(tr) + Pl + Fe
1122	− 13.53	48	Ol + Ar(tr) + Cp + Pg + Il + Pl + Fe

*Reversal runs, both held at 1161°C, − 13.00 (assemblage was Sp + Ol + Ar + Fe + L) for 24 hr prior to temperature and oxygen fugacity change.

Sp—spinel; Ol—olivine; Ar—armalcolite; Il—ilmenite; Cp—clinopyroxene; Pg—pigeonite; Pl—plagioclase; Fe—metallic iron; tr—trace.

Phase Relations

The results of the constant temperature experiments (Table 1) are graphically depicted in Fig. 1. Metallic iron and spinel appear on the liquidus at about 0.5 log units below the iron-wüstite buffer (IW). Liquidus iron is stable in our experiments and probably stable in the natural basalts, primarily expressed as an Fe–FeS immiscible liquid (sulfur is lost in our experiments). Chromian–ulvöspinel ceases to be a liquidus phase at about 2 log units below IW if the spinel out curve is extrapolated from lower temperature points. The crystallization temperature of olivine is suggested to increase with decreasing oxygen fugacity due to the precipitation of increasing amounts of metallic iron causing the liquid to be more magnesium rich and the olivine more forsterite rich. Armalcolite is the next phase to precipitate with falling temperature. Its temperature of appearance is interpreted to decrease slightly with decreasing oxygen fugacity possibly due to more chromium, as Cr^{2+}, and trivalent titanium being incorporated.

Plagioclase, pyroxene (augite and/or pigeonite) and ilmenite crystallize within a 10–15°C temperature interval and the sequence of appearance is critically

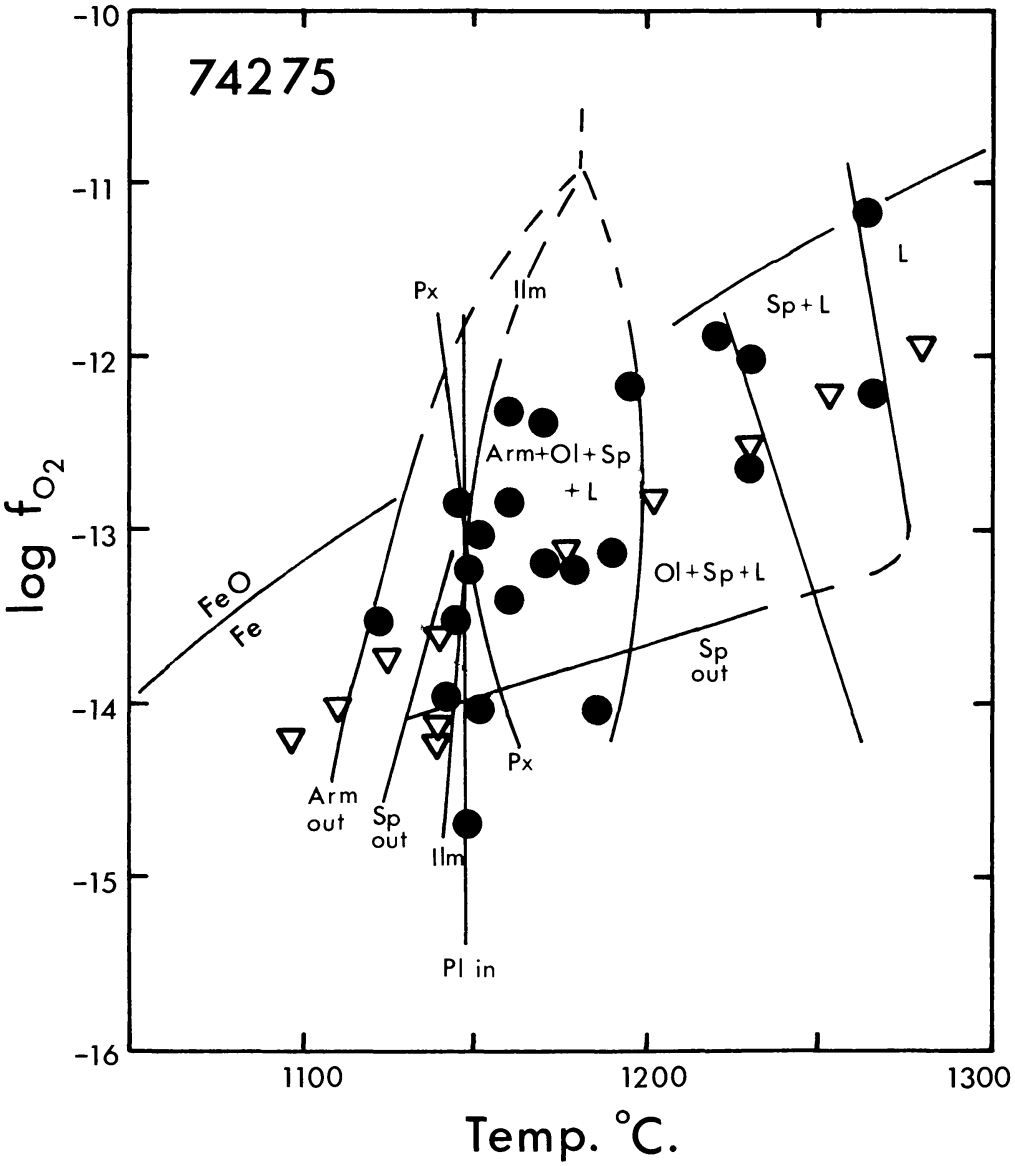

Fig. 1. Melting relations of 74275,109. Triangular points are those of O'Hara and Humphries (1975) at their stated oxygen fugacities. The iron-wüstite (Fe–FeO) buffer curve is shown as reference. Uncertainties in temperature and f_{O_2} are the same as shown in Fig. 2.

dependent on oxygen fugacity. This temperature interval is depicted in an expanded form in Fig. 2. The crystallization of plagioclase shows no dependency on oxygen fugacity within the investigated range. Ilmenite decreases its temperature of appearance under progressively more reducing conditions, whereas pyroxene increases its temperature of appearance. Pigeonite crystallizes at increasing temperatures with decreasing oxygen fugacity. It is difficult, however, to accurately determine the pigeonite relation within this narrow temperature-f_{O_2} interval. Spinel reacts out of the system with falling temperature and is unstable at very reducing conditions. Armalcolite reacts out within the range of lunar oxygen

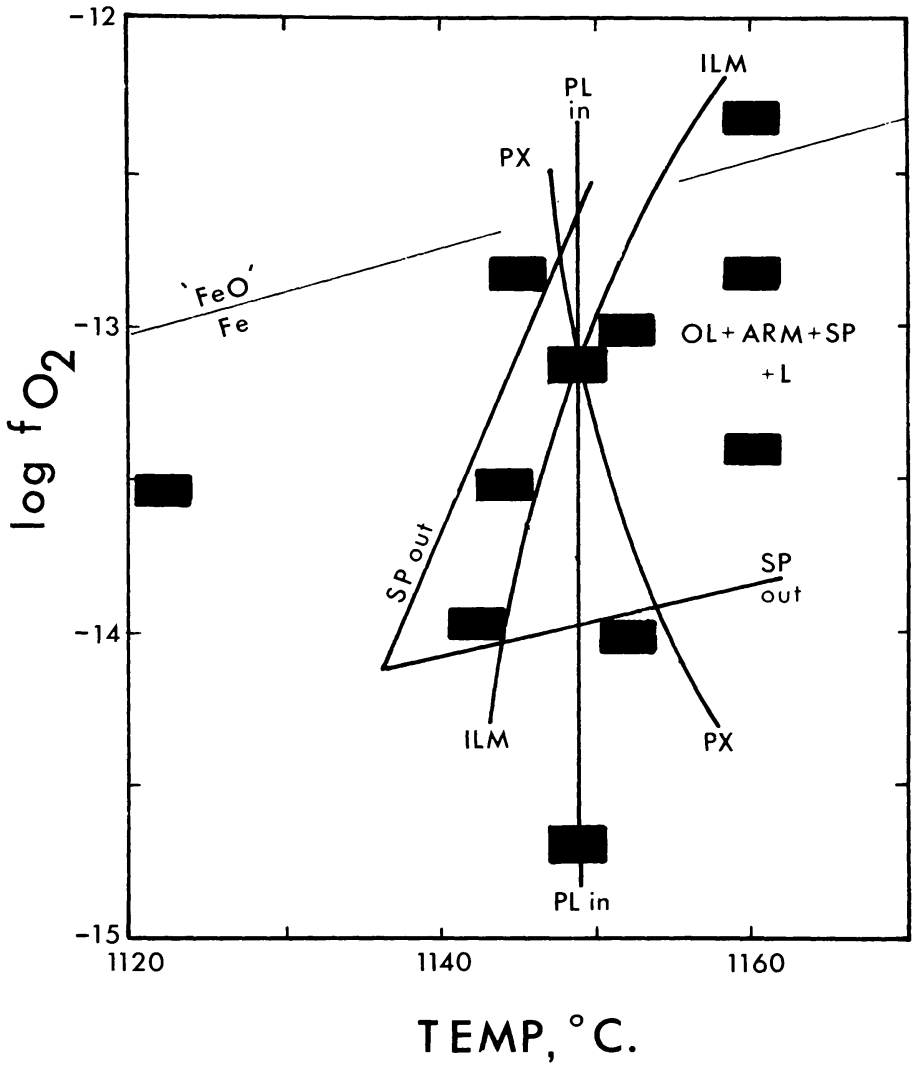

Fig. 2. Melting relations of an expanded portion of Fig. 1, suggesting the reversal of pyroxene and ilmenite appearance with falling temperature. The size of the data boxes are the estimated magnitude of the uncertainties in T°C and f_{O_2}.

fugacity about 30°C after ilmenite appears. The crystallization curves of pyroxene and ilmenite intersect approximately at one point, which coincides with the appearance of plagioclase, at about 0.4 log units below IW and at about 1148°C. The data of O'Hara and Humphries (1975) are in agreement at their cited oxygen fugacity values and are represented on Fig. 1 as open triangles. Because the oxygen fugacity for runs in iron capsules is unknown, the data of Green *et al.* (1975) cannot be shown in Fig. 1.

Because the pyroxene and ilmenite curves are interpreted to cross, the order of appearance of pyroxene and ilmenite can be reversed as a function of oxygen fugacity. The textures of the cooling experiments provide striking evidence for the reversal in the order of appearance of pyroxene and ilmenite (see textures section).

TEXTURES

The textures in the cooling runs (Table 2) varied as a result of the complex interplay between the oxygen fugacity, the cooling rate and history, and the nucleation kinetics of the different phases, primarily plagioclase (Figs. 3, 4a, and 4c). The most dramatic effect of variation in the values of oxygen fugacity is to reverse the order of appearance of ilmenite and pyroxene, shown in two charges cooled at the same rate but with different oxygen fugacity paths showing strikingly different textures (Figs. 3a and b). For those runs which had f_{O_2} paths near IW, the ilmenite occurs as large parallel plates (Figs. 3a and 4b) and obviously crystallized first, unhindered by pyroxene. These ilmenite plates are presumably connected in the third dimension to form single crystal (suggested by their extinction characteristics). These plates only occur if the liquid is free of turbulence (Usselman *et al.*, 1975) and such orientations are rarely observed in the natural high-Ti basalts. For the runs that had f_{O_2} paths as little as 0.5 log units below IW and lower (Figs. 3b, 3c, 3d, and 4a), the ilmenite occurs as individual crystals (randomly oriented). Texturally, it appears that the ilmenite and pyroxene may have co-crystallized, but the appearance of pyroxene before ilmenite is definitely suggested in Fig. 3c.

The effects of cooling rate on the textures are obvious; the slower cooling rates produce coarser-grained textures (cf. Figs. 4c, 3a, and 3c). It is apparent, however, that the interplay of the effects of different oxygen fugacity on the order of appearance of the phases with cooling rate can produce significantly different grain sizes for runs cooled at similar rates (cf. X-23, Fig. 3a and X-24, Fig. 3b). The nucleation of plagioclase at the lower f_{O_2} of X-24 and its absence in X-23 also alters the appearance of the texture. The interplay of cooling rate and nucleation kinetics in X-22 produced marked variations in grain size within a single charge (Fig. 4c). Areas with coarser-grained augite occur as isolated patches within a matrix whose augite is much finer and often occurs as fan spherulites. This feature is very similar to segregations in 70215 (Fig. 4d).

The textures in the partially melted runs (X-25, Fig. 3d and X-26, Fig. 4a)

Table 2. Run conditions of cooling experiments.

Run no.	Melt T, °C	Final T, °C	$\Delta \log f^*_{O_2}$	Cooling rate
22	1280	1031	0	7°C/hr
23	1280	960	0	1.8°C/hr
24	1280	980	−1.25	1.8°C/hr
25	1170	960	−1.0	2°C/hr
26	1170	980	−0.5	7°C/hr
27†	1270	1160	−0.5	0.9°C/hr
	1160	1110	−0.5	7°C/hr

*The oxygen fugacity of each run is nearly parallel to the iron-wüstite buffer curve; the number in this column indicates the fractions of log units below the I-W curve.

†Two-stage cooling history.

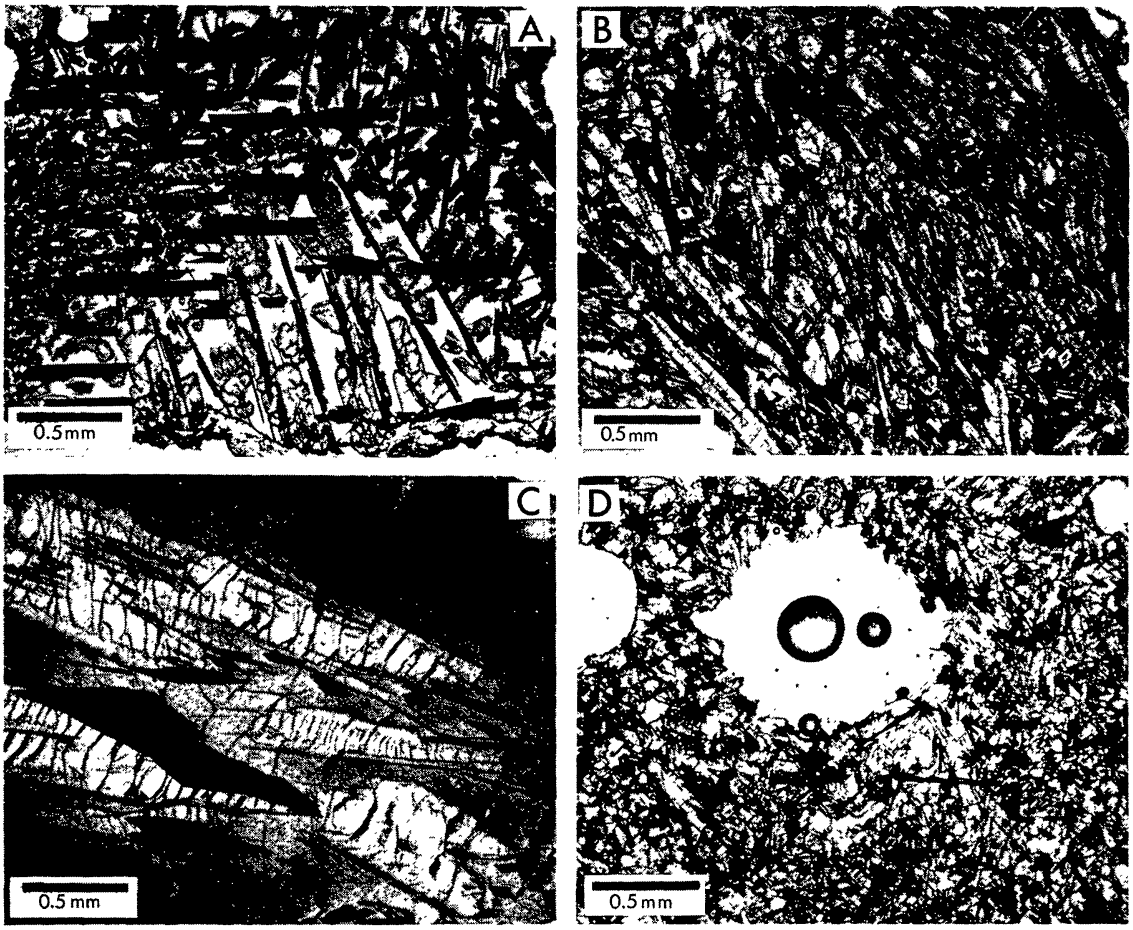

Fig. 3. Photomicrographs of experimentally produced basalts crystallized from a powered fraction of 74275. (a) Run X-23 (1.8°/hr, $f_{O_2} \sim$ IW) showing ilmenite dendrites that crystallized before pyroxene and a glassy matrix. (b) Run X-24 (1.8°/hr, $f_{O_2} \sim$ IW − 1.25 log units) showing elongate pyroxene that crystallized before ilmenite. (c) Run X-27 (0.9°/hr to 1160°C; 7°/hr to 1110°C, $f_{O_2} \sim$ IW − 0.5 log units) showing large pigeonite crystals rimmed by augite and ilmenite. (d) Run X-25 showing textures resulting from partial melting then crystallization at 2°/hr ($f_{O_2} \sim$ IW − 1.0 log units).

provide an interesting contrast to the textures that developed from an entirely liquid precursor (X-22, 23, and 24). In both runs pyroxene appeared before ilmenite due to the oxygen fugacity. The differences in cooling rate of 5°C/hr between the two charges is not readily apparent and plagioclase has apparently readily nucleated in both. In general, the crystals in X-25 and X-26 are more equant and homogeneous than in the completely melted charges. The olivine is most notably different. In the partially melted runs where olivine is a residual phase, it is nearly equant and anhedral, while in the completely melted runs where olivine grew from the melt it is skeletal and usually elongate.

The textures in X-25 and especially X-26 (Figs. 3d, 4a) are remarkably similar to 74275 (Fig. 4b). The olivine crystals in both the experimental and natural basalts are anhedral, equant, and fractured in a similar manner. The olivine in the experimental basalts are smaller, but their size is a function of the grinding of the

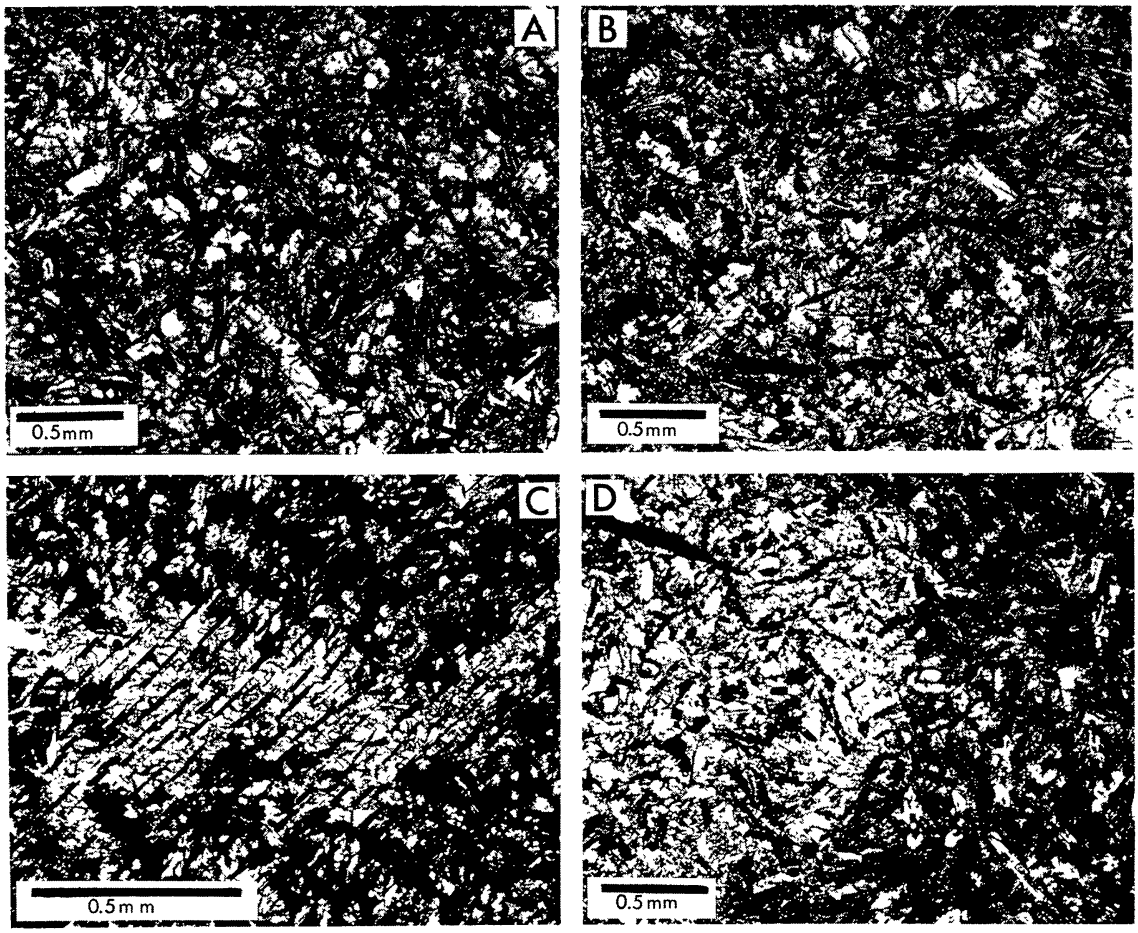

Fig. 4. Photomicrographs of experimentally crystallized 74275 compared to the natural rock. (a) Run X-26 showing the texture that resulted from partially melting then cooling at 7°C/hr ($f_{O_2} \sim$ IW − 0.5 log units). (b) 74275,89 showing the texture of the natural rock and the close correspondence between it and the experimentally produced basalt. (c) Run X-22 (7°/hr, $f_{O_2} \sim$ IW) showing a heterogeneous texture of coarser-grained pyroxene enclosed in a matrix of fan-spherulitic pyroxene. (d) 70215,147 showing a similar texture to X-22 except for the slightly larger grain size and circular shapes of the coarser-grained pyroxene.

original material and not the process which formed the olivines in 74275. The pyroxene, plagioclase, armalcolite, spinel, and ilmenite in X-26 most closely resemble grain sizes and morphologies in 74275.

PHASE CHEMISTRY

Liquid

The composition of the liquid fractions from the constant temperature experiments parallels the liquid line of descent determined by Longhi *et al.* (1974) for other high-titanium compositions. Because 72475 is more magnesium rich than the other Apollo 17 basalts (Rhodes *et al.*, 1976), our experimental liquid line of

descent is also more magnesium rich than the trends cited above. The trend (using TiO_2 vs. Mg/(Mg + Fe)) nearly coincides with the calculated liquid line of descent of Rhodes *et al.* (1976) for their high-Rb basalt group (74255, 74245, and 74275), but is offset towards higher Mg/(Mg + Fe) than the high-Rb basalts because of the iron loss. Because the iron loss is less severe in the temperature range involving pyroxene, ilmenite, and plagioclase crystallization, our lower temperature liquid compositions (Fig. 5) fall on the extrapolated liquid line of descent (Rhodes *et al.*, 1976) for the high-Rb high-titanium basalts. The fact that spinel is the liquidus phase has very little effect on the general nature of the fractionation trends. Our experimental liquid line of descent only includes experimental points that were run between IW and 0.5 log units below IW. At lower oxygen fugacities the liquid became even more magnesium rich due to precipitation of large amounts of metallic iron.

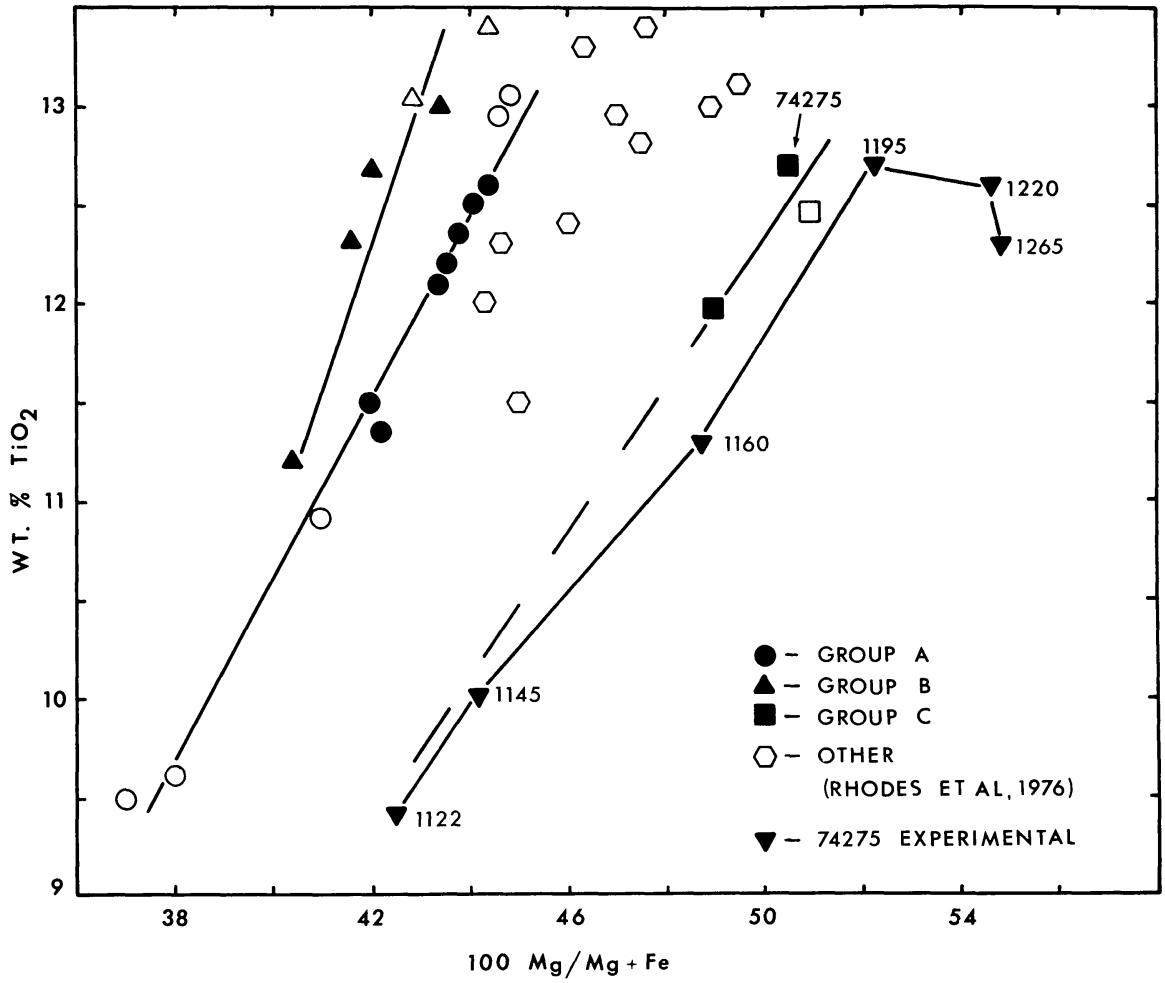

Fig. 5. Liquid line of descent of selected constant temperature runs on 74275,109 near the IW buffer plotted in relationship to the chemical classification of Rhodes *et al.* (1976). Our curve is offset to higher 100 Mg/(Mg + Fe) due to iron loss to the Pt-wire loop.

Olivine

Olivine chemistry cannot be rigorously treated because of the iron loss problem. Olivine compositions, however, do fall in the range observed in 74275. In the constant temperature experiments, olivine liquid has a distribution coefficient ($K_D = (FeO)_{OL} \cdot (MgO)_{LIQ}/(FeO)_{LIQ} \cdot (MgO)_{OL}$) between 0.28 and 0.31. This K_D is slightly temperature dependent, similar to that noted by Green *et al.* (1975). Longhi *et al.* (1975) have noted that the presence of 7–11 mole% TiO_2 in lunar basalts lowers the K_D from 0.33 (for low Ti-basalts) to values in the range 0.26–0.29. Our K_D is slightly higher than that of Longhi *et al.*, which may be attributable to their Fe-capsule technique (i.e., is the f_{O_2} of the iron capsules in a realistic range for lunar crystallization?). The chromium content of the olivines has an interesting relationship as a function of oxygen fugacity. Figure 6 shows the Cr_2O_3 content vs. mole% forsterite in the constant temperature runs. The content of chrome in the olivine increases at lower f_{O_2} values within the phase field of olivine, armalcolite, spinel, and liquid. This suggests an increase in the amount of divalent chromium in the melt with lower f_{O_2}. Schreiber and Haskin (1976) observed similar chrome behavior in experiments on synthetic systems.

In the cooling experiments the olivine composition is controlled largely by the

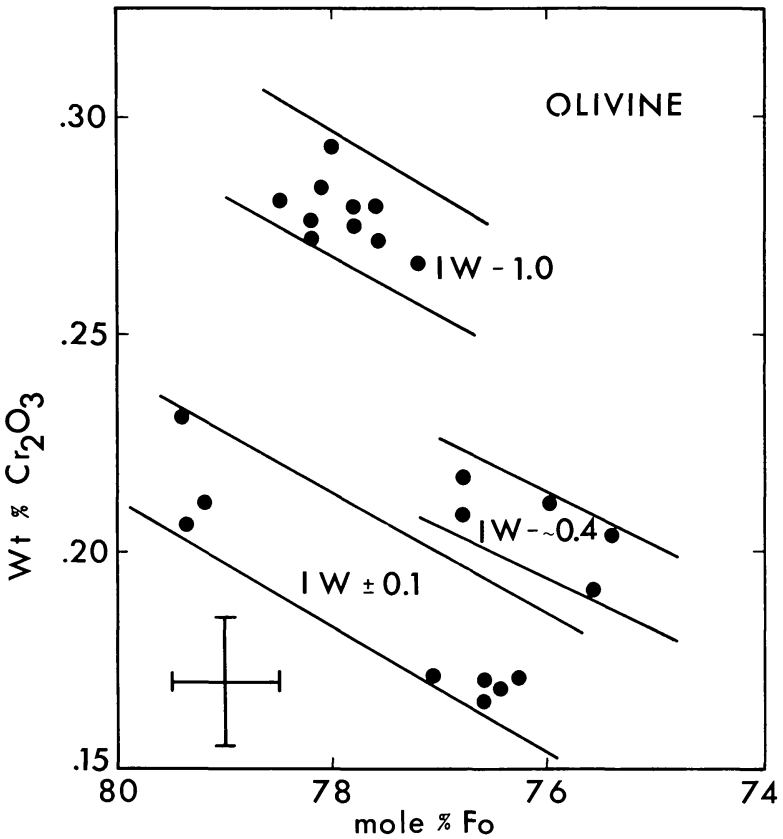

Fig. 6. Variation of chromium content (wt.% Cr_2O_3) of olivine as a function of forsterite content and Δf_{O_2} relative to the IW buffer. Uncertainties are indicated in lower left-hand corner.

oxygen fugacity. If the oxygen fugacity is near IW (X-23), the olivines are Fo_{75-80}. If the oxygen fugacity is significantly below IW (X-24), large amounts of metallic iron precipitate and the olivine is about Fo_{90}. The olivines in the partially melted runs (X-25 and X-26) retain their original composition, but do show some reaction with the melt or enclosing pyroxene. A single grain may show as much as a Fo_{6-7} decrease from core to rim. Olivine has totally reacted out of the system at 1°/hr.

Armalcolite

Armalcolite occurs in every run below 1195°C. With falling temperature, Fe/(Fe + Mg) shows very little variation within a given phase field. Within the armalcolite + olivine + spinel + liquid field, armalcolite liquid has a distribution coefficient $((FeO)_{ARM} \cdot (MgO)_{LIQ}/(FeO)_{LIQ} \cdot (MgO)_{ARM})$ of 0.83 ± 0.02. However, with the appearance of ilmenite and pyroxene in the Ol + Sp + Arm + L field there is a large change in Fe/(Fe + Mg) (Fig. 7) of armalcolite toward iron enrichment. This iron enrichment of the armalcolite co-precipitating with ilmenite is opposite than one would predict from the $MgTi_2O_5$–$FeTi_2O_5$ equilibrium relations (Lindsley *et al.*, 1974) and was termed an armalcolite "suicidal" trend by Papike *et al.* (1974). The "suicidal" armalcolite trend may result from the co-precipitation of pyroxene which may override a magnesium enrichment of the armalcolite by ilmenite as predicted from the $MgTi_2O_5$–$FeTi_2O_5$ system. The MgO contents (wt.%) of the

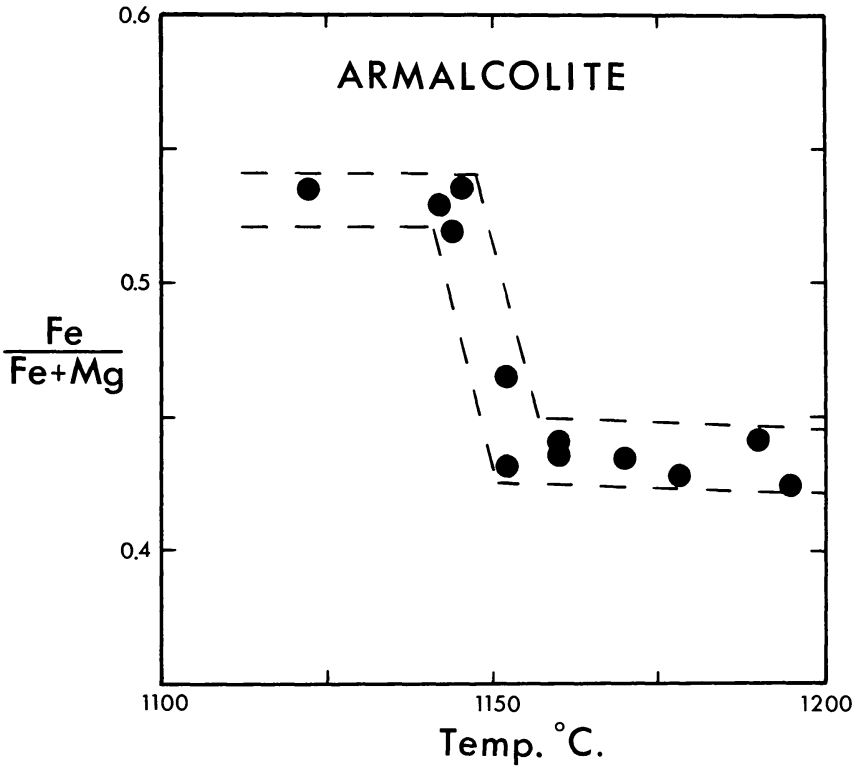

Fig. 7. The variation of Fe/(Fe + Mg) in armalcolite as a function of temperature. This variation is independent of oxygen fugacity and shows a rapid change correlated with the appearance of ilmenite and pyroxene.

co-existing armalcolite and ilmenite are virtually identical. Chromium shows a similar change, with decreasing chromium, which can be correlated with the appearance of ilmenite and pyroxene although it is not as pronounced as the change in Fe/(Fe + Mg). The ilmenite in this case is slightly more enriched in Cr_2O_3 than the co-existing armalcolite. The ilmenite in the natural high-Ti basalts is always poorer in Cr_2O_3 than armalcolite, and one must resort to equilibration of the chrome (and MgO) content of the ilmenite with falling temperatures, as suggested by Usselman (1975).

If the armalcolite analyses are recast to give the ideal structural formula of 3 cations/5 oxygens and assuming all the chromium is trivalent, then all of the experimentally grown armalcolites contain trivalent titanium, similar to those observed by Wechsler *et al.* (1975). The amount of trivalent titanium is primarily dependent on the oxygen fugacity. Figure 8 and Table 3 show the $Ti^{3+}/(Ti^{3+} + Ti^{4+})$ of the experimental armalcolites, relative to the oxygen fugacity of the run. The iron-wüstite buffer is used as a reference to eliminate the temperature dependency of the oxygen fugacity. The spread of the experimental points shows that the amount of Ti^{3+} is relatively insensitive to temperature (Table 3), however, the lower temperature armalcolites do tend to show slightly less Ti^{3+} than the higher temperature armalcolites crystallized at the same relative oxygen fugacity. The effect of all of the chromium being divalent would shift the field in Fig. 8 to lower values of 100 $(Ti^{3+}/(Ti^{3+} + Ti^{4+}))$ by approximately 4 units. If all the chromium is divalent and stoichiometry is assumed, there is still trivalent titanium in all of the armalcolites.

The natural armalcolites in high-titanium mare basalts show a range of 100 $(Ti^{3+}/(Ti^{3+} + Ti^{4+}))$ indicative of an oxygen fugacity between the iron-wüstite buffer and approximately 1 log unit below IW. These implied values are within the measured range of oxygen fugacity for high-titanium mare basalts (Sato, 1976). The values of f_{O_2} are also commensurate with those implied using the criteria of ilmenite crystallizing before pyroxene or *vice versa* (Fig. 2).

Spinel

The spinel compositions from the constant temperature experiments on 74275,109 are typical of high-titanium mare basalts and are intermediate between ulvöspinel and chromite, with 15–20 mole% aluminous spinel component. The trend with falling temperature is the same as that observed in zoned chromian ulvöspinels from the high-titanium mare basalts (El Goresy *et al.*, 1974). There was no observed systematic variation of composition with differences in oxygen fugacity with the exception of the calculated Cr^{2+} content.

If the spinel compositions are recalculated to give the ideal spinel structural formula of 24 cations/32 oxygens and assuming all the titanium as Ti^{4+}, all of the experimental spinels contain some divalent chromium. The construction of an oxygen geobarometer was attempted, similar to that constructed for Ti^{3+} in armalcolite, however, it was found that the $Cr^{2+}/(Cr^{2+} + Cr^{3+})$ was compositional and/or temperature dependent, and the Cr^{2+} content of *spinels cannot be used as an oxygen geobarometer.*

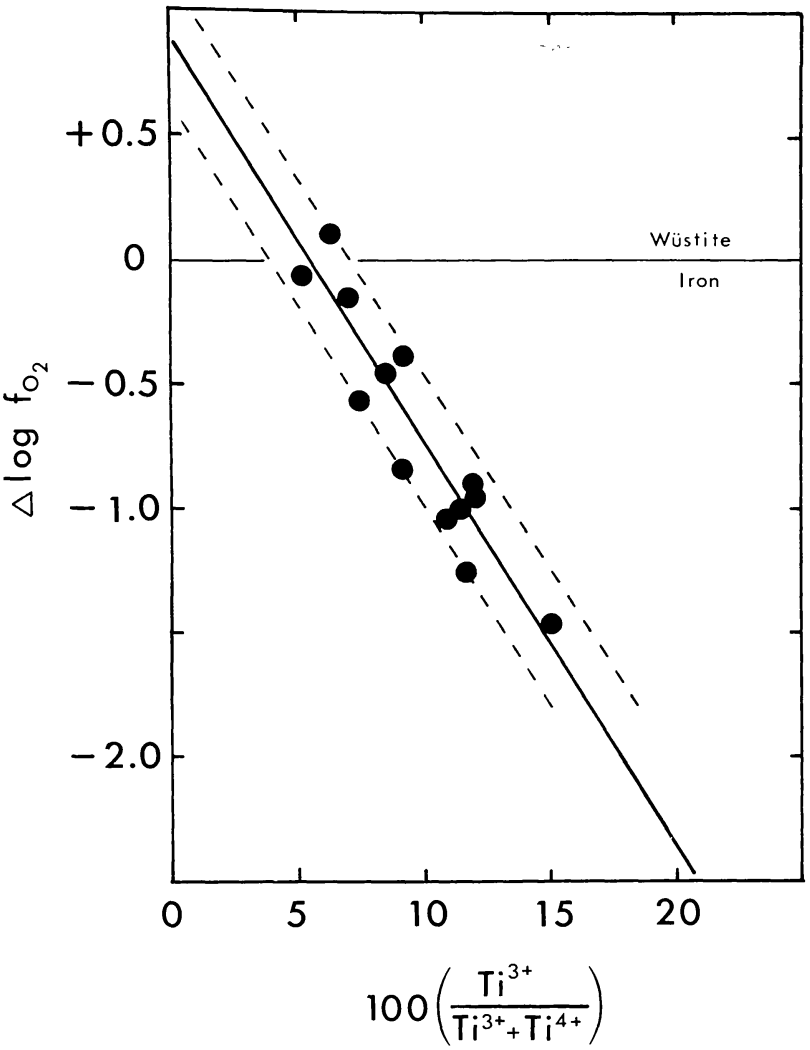

Fig. 8. Variation of Ti^{3+} content of armalcolite with f_{O_2}. The solid line is the linear least squares fit and the dashed lines represent one σ. All of the points (Table 3) were measured under identical conditions on the microprobe on the same day.

Pyroxene

The pyroxenes in the constant temperature experiments are both pigeonite and augite at oxygen fugacities greater than 0.5 log units below IW, while under slightly more oxidizing conditions, augite is probably the only pyroxene until near-solidus temperatures. With falling temperature the pigeonite becomes enriched in FeO, while the co-existing augite becomes slightly enriched in CaO with increasing FeO. The chemical trends (Fig. 9) with falling temperature are more adequately displayed by the pyroxenes in the cooling rate experiments.

The pyroxenes grown in the cooling experiments show a wide variety of zoning patterns which reflect differences in oxygen fugacity and cooling rate. The effect of oxygen fugacity is the same as for olivine. At f_{O_2} values greater than 1 unit below IW, metallic iron precipitates depleting the melt and the pyroxene in Fe relative to Mg. Runs X-24 and X-25 show this effect most clearly. Pyroxenes grown at higher f_{O_2} values generally have higher Fe to Mg ratios and less zoning in

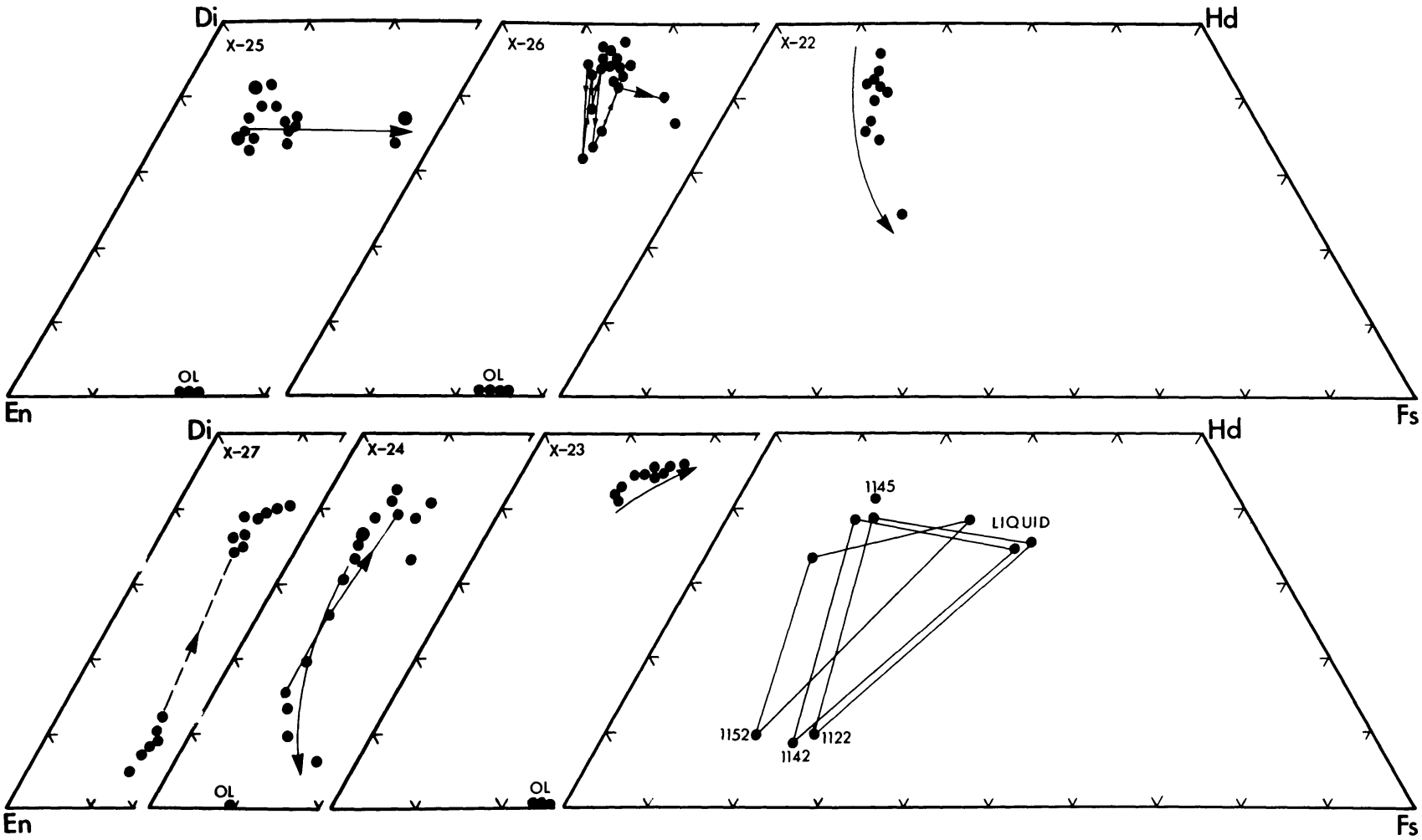

Fig. 9. Compositions of the pyroxenes and olivines from the cooling and constant temperature runs plotted on the pyroxene quadrilateral (see text for details). The three constant temperature runs where pigeonite, augite, and liquid co-exist are shown in the lower right diagram. The point at 1145° is for an augite grown near the IW buffer where pigeonite does not occur.

Table 3. Titanium (3+) content of armalcolites experimentally crystallized from 74275,109. Iron-wüstite buffer values are calculated from Williams (1971).

Temperature, °C	$-\log f_{O_2}$	$\Delta \log f_{O_2}$ (IW)	$\left[\frac{Ti^{3+}}{Ti^{3+}+Ti^{4+}}\right]100$
1195	−12.17	−0.16	7.51
1190	−13.12	−1.05	10.85
1178	−13.23	−1.01	11.50
1170	−12.39	−0.07	5.02
1170	−13.19	−0.87	12.07
1160	−12.32	+0.13	6.55
1160	−12.83	−0.38	9.16
1160	−13.40	−0.95	12.06
1152	−13.01	−0.45	8.85
1152	−14.02	−1.46	15.02
1144	−13.51	−0.85	9.12
1142	−13.97	−1.28	11.60
1122	−13.53	−0.57	7.54

a given crystal, e.g., X-22 and X-23; the apparent extended zoning range in X-22 results from combining analyses of several different crystals. Pigeonite crystallized at the lower f_{O_2} values (X-27 and X-24), but its presence may be primarily controlled by cooling rate.

Pyroxene crystals grown at different cooling rates show remarkably different zoning patterns. The most extensively zoned crystals occur in X-27 as a result of the very slow cooling rate (Fig. 9). The crystals have large, modestly-zoned pigeonite cores up to 4 mm by 1 mm and are rimmed by subcalcic augite, up to 250 μ (Fig. 3c). The augite shows oscillatory zoning. The pigeonite in X-24 is not well developed. It occurs either as very thin rims on augite crystals or as intermediate compositions in olivine-cored crystals that zone outward to augite (Fig. 9). In both of these runs, augite has nucleated *independent* of pigeonite or olivine, and in X-24 is zoned toward pigeonite.

The pyroxenes grown from the liquid in the run that were partially melted (X-25 and X-26) show fine scale oscillatory zoning (Fig. 9). The oscillations are primarily in Ca content for the more rapidly cooled X-26 and in Mg to Fe ratio for the more slowly cooled X-25. No pigeonite was found in X-25 even though it cooled at rates comparable to X-27 and X-24.

Discussion

The sequence of crystallization between pyroxene and ilmenite has been interpreted above to be critically dependent on the oxygen fugacity. This dependency occurs within the estimated range of lunar oxygen fugacities of high-titanium mare basalts (Sato, 1976), between the iron-wüstite buffer and 1 log unit below IW. With this dependency, which has been shown to be independent of cooling rate, and with the interpretations of El Goresy *et al.* (1974) of different

pyroxene-ilmenite paragenesis for Apollo 17 basalts, the range of oxygen fugacity of crystallization of these high-titanium basalts can be estimated. In addition to the estimates based on crystallization sequence, oxygen fugacity can also be estimated using the experimentally determined $Ti^{3+}/(Ti^{3+} + Ti^{4+})$ content of armalcolites (Fig. 8). These two estimates of f_{O_2} appear consistent for the limited number of samples tested. 70017 and 70035 exhibit pyroxene crystallizing before ilmenite and have armalcolites with Ti^{3+} contents indicative of crystallization at approximately 0.6–0.7 log units below IW. This f_{O_2} value is within the range where pyroxene crystallizes before ilmenite. Ilmenite crystallizes before pyroxene in 70215 and 74275 and their armalcolites have Ti^{3+} contents suggestive of an oxygen fugacity about 0.2–0.3 log units below IW. This oxygen fugacity is consistent with both techniques of estimation.

Sato (1976) has measured the intrinsic oxygen fugacities of 70017 and 74275 using the double cell technique and arrived at essentially the same two oxygen fugacity ranges as suggested above.

Samples 70017 and 70035, which apparently crystallized pyroxene before ilmenite and represent the more "reduced" Apollo 17 mare basalts, may be chemically classified as olivine enriched samples of the type A basalt of Rhodes *et al.* (1976), as shown on Fig. 5. 70215, 74275 and the bulk of the samples classified in Rhodes *et al's* type A, B, and C basalts crystallized ilmenite before pyroxene and represent the more "oxidized" high-titanium basalts. If 70017 and 70035 represent olivine enriched variants of type A basalt, how do they exhibit different apparent oxygen fugacities from the type A basalts?

It is possible that the oxygen fugacity during crystallization is externally buffered by a gaseous species rather than internally buffered. From the calculations of Gerlach (1974) on the composition of a possible lunar basalt gaseous species, this gas may be enriched in hydrogen relative to other buffering gases. The retention of these gases would lead to a more reduced crystallization sequence, while outgassing would result in slightly more oxidized samples. As the difference between the reduced and oxidized samples is small, the amount of buffering gases would probably be small. The retention of these gases would be possible if the basalt was emplaced as a shallow sill or in the center of a thick flow. Loss of these gases could occur during surface extrusion or the preferential diffusion of hydrogen through microfractures and cracks prior to emplacement (Sato, pers. comm.).

The texture of 74275 is very closely replicated by the partially melted run X-26 that cooled at 7°C/hr. This compares very well with the prediction of Usselman *et al.* (1975) of 5–10°C/hr based on cooling experiments using synthetic compositions that are only generally similar to 74275. The estimate was based on ilmenite morphology, which appears to be closely tied to specific cooling rates for all the titanium-rich basalts.

The fact that the partial melt history was necessary to reproduce the 74275 texture implies strongly that olivine, spinel, armalcolite and Fe° were present in these lavas upon eruption.

Walker *et al.* (1976b) have described textures in 70215 and 74275 that resemble

the texture produced experimentally in X-22 (cf. Figs. 4c and 4d). We have not checked for the compositional differences that Walker *et al.* observe, but the relative morphologies and sizes of the phases are similar. Walker *et al.* (1976b) propose two possible origins: one based on previously crystallized material settling into a melt of slightly different composition and a second, which they seem to favor, based on nucleation and growth effects that result from rapid cooling. The nature of our experiments precludes the mixing of previously crystallized material and a melt. We, therefore, support the nucleation and growth model.

This heterogeneous texture may form by a mechanism similar to that proposed for the development of porphyritic textures at linear cooling rates (Lofgren *et al.*, 1974; Dowty *et al.*, 1974; Lofgren and Donaldson, 1975). Plagioclase and pyroxene appear at approximately the same temperature. If the pyroxene nucleation takes place at the appropriate temperature or at some modest supersaturation, nucleation will be sparse and the crystals will grow fairly large. If the cooling rate is sufficiently rapid so that plagioclase nucleation is delayed and pyroxene crystallization cannot keep up with the temperature decrease, the remaining liquid will become increasingly supersaturated with respect to plagioclase and pyroxene. When the melt is sufficiently supersaturated, nucleation will be massive and growth rapid so that the crystals will be smaller and have morphologies typical of rapid growth. These shapes are commonly the fan spherulitic (variolitic) intergrowths of pyroxene and plagioclase. If this process occurs during eruption and flow, the early crystallized coarser pyroxene will tend to form clusters that assume rounded shapes and be enclosed in a matrix of finer material as observed by Walker *et al.* (1976b). Obviously, our experimental charges did not flow and the coarse-grained patches are not rounded. The domain texture occurs only in runs crystallized from a total liquid, however, we are not justified to conclude at the present time that these domains are indicative of crystallization only from a total liquid.

Some limits can be placed on phenomena that appear to be dependent on cooling rate. The limits are not very rigorous because of the limited number of experiments performed. Some of the phenomena could be explored further on synthetic material. Brown *et al.* (1975) suggest that the percent of modal olivine is cooling rate dependent. We do see a relationship with presence of olivine and cooling rate (similar to that noted in a synthetic Apollo 15 quartz-normative basalt by Lofgren *et al.*, 1974). Olivine is absent at 1°C/hr, even though 74275 is richer in normative olivine than most Apollo 17 rocks. Pigeonite is rare in Apollo 17 rocks and our experiments suggest that cooling rate would have to be less than 1°C/hr and the f_{O_2} approximately 1 log unit below IW for pigeonite to be significant. Plagioclase nucleation is reluctant (Gibb, 1975; Usselman *et al.*, 1975) in basalts generally and even in these very fluid lunar compositions. We suspect that the pyroxene may be especially Ca-rich because plagioclase does not nucleate at its equilibrium temperature. The subsequent growth of Ca-rich pyroxene or Ti-rich pyroxene (Nash and Haselton, 1975) may then further suppress plagioclase nucleation. The relative ease of plagioclase nucleation in experiments which were

partially melted (plagioclase-absent) is not understood and further work on a variety of basaltic compositions is currently underway to attack this problem.

CONCLUSIONS

Our experiments, both at constant temperature and continuous cooling, have shown the following features:

(1) The melting relations are sensitive to *very small* changes in oxygen fugacity within the lunar range. This is well displayed by the pyroxene-ilmenite paragenesis, implied both by constant temperature and continuous cooling experiments (Figs. 2, 3a, 3b).

(2) The Ti^{3+} content of armalcolite varies as a function of f_{O_2} (Fig. 8). The oxygen fugacity values estimated using the Ti^{3+} contents and the pyroxene-ilmenite paragenetic sequence for the basalts are consistent.

(3) The comparison of the basalt chemistry (Rhodes *et al.*, 1976) and the estimated oxygen fugacity implies that a gaseous buffer may have been present in the basalts prior to eruption. Most of the buffering gas escaped during extrusion and flow, however some samples appeared to have retained these gases during their solidification history.

(4) The cooling rate experiments on 74275,109 indicate that cooling rate estimates of Usselman *et al.* (1975) based on ilmenite morphology is independent of composition. However, the general textures developed during cooling are shown to be a complex interaction of cooling rate, oxygen fugacity and nucleation kinetics.

(5) Cooling experiments on 74275 indicate that upon eruption it contained olivine, spinel, armalcolite, metallic iron, and approximately 80% liquid. Subsequent crystallization took place at 5–10°C/hr and an oxygen fugacity 0.3 to 0.4 log units below and approximately parallel to the iron-wüstite buffer.

Acknowledgments—The authors wish to acknowledge helpful reviews by D. H. Lindsley and J. Longhi. A portion of the research reported in this paper was done while one of the authors (TMU) was a Visiting Post-Doctoral Fellow at the Lunar Science Institute, which is operated by the Universities Space Research Association under Contract No. NSR-09-051-001 with the National Aeronautics and Space Administration. This paper constitutes the Lunar Science Institute Contribution No. 249.

REFERENCES

Bence A. E. and Albee A. L. (1968) Empirical correction factors for the electron microanalysis of silicates and oxides. *J. Geol.* **76**, 382–403.

Brown G. M., Peckett A., Emeleus C. H., Phillips R., and Pinset R. H. (1975) Petrology and mineralogy of Apollo 17 mare basalts. *Proc. Lunar Sci. Conf. 6th*, p. 1–13.

Donaldson C. H., Usselman T. M., Williams R. J., and Lofgren G. E. (1975a) Experimental modeling of the cooling history of Apollo 12 olivine basalts. *Proc. Lunar Sci. Conf. 6th*, p. 843–869.

Donaldson C. H., Williams R. J., and Lofgren G. E. (1975b) A sample holding technique for study of crystal growth in silicate melts. *Amer. Mineral.* **60**, 324–326.

Dowty E., Keil K., and Prinz M. (1974) Lunar pyroxene-phyric basalts: Crystallization under supercooled conditions. *J. Petrol.* **15**, 419–453.

El Goresy A., Ramdohr P., Medenbach O., and Bernhardt H. (1974) Taurus-Littrow TiO_2-rich basalts: Opaque mineralogy and geochemistry. *Proc. Lunar Sci. Conf. 5th*, p. 627–652.

Gerlach T. M. (1974) "The C–O–H–S gas system and its application to terrestrial and extraterrestrial volcanism." Ph.D. dissertation, University of Arizona, Tucson, Arizona.

Gibb F. G. F. (1974) Supercooling and the crystallization of plagioclase from a basaltic melt. *Mineral. Mag.* **39**, 641–653.

Green D. H., Ringwood A. E., Hibberson W. O., and Ware N. G. (1975) Experimental petrology of Apollo 17 mare basalts. *Proc. Lunar Sci. Conf. 6th*, p. 871–893.

Lindsley D. H., Kesson S. E., Hartzman M. J., and Cushman M. K. (1974) The stability of armalcolite: Experimental studies in the system MgO–Fe–Ti–O. *Proc. Lunar Sci. Conf. 5th*, p. 521–534.

Lofgren G. E. and Donaldson C. H. (1975) Phase relations and non-equilibrium crystallization of ocean ridge tholeiite from the Nazca plate (abstract). *EOS (Trans. Amer. Geophys. Union)* **56**, 468.

Lofgren G. E., Donaldson C. H., and Usselman T. M. (1975) Geology, petrology, and crystallization of Apollo 15 quartz-normative basalts. *Proc. Lunar Sci. Conf. 6th*, p. 79–99.

Lofgren G., Donaldson C. H., Williams R. J., Mullins O., Jr., and Usselman T. M. (1974) Experimentally reproduced textures and mineral chemistry of Apollo 15 quartz normative basalts. *Proc. Lunar Sci. Conf. 5th*, p. 549–567.

Longhi J., Walker D., Grove T. L., Stopler E. M., and Hays J. F. (1974) The petrology of the Apollo 17 mare basalts. *Proc. Lunar Sci. Conf. 5th*, p. 447–469.

Longhi J., Walker D., and Hays J. F. (1975) Fe–Mg distribution between olivine and lunar basaltic liquids (abstract). *EOS (Trans. Amer. Geophys. Union)* **56**, 471.

Nash W. P. and Haselton J. D. (1975) Silica activity in lunar lavas. *Proc. Lunar Sci. Conf. 6th*, p. 119–130.

O'Hara M. J. and Humphries D. J. (1975) Armalcolite crystallization, phenocryst assemblages, eruption conditions and origin of eleven high titanium basalts from Taurus-Littrow (abstract). In *Lunar Science VI*, p. 616–618. The Lunar Science Institute, Houston.

Papike J. J., Bence A. E., and Lindsley D. H. (1974) Mare basalts from the Taurus-Littrow region of the moon. *Proc. Lunar Sci. Conf. 5th*, p. 471–504.

Rhodes J. M., Hubbard N. J., Wiesmann H., Rodgers K. V., Brannon J. C., and Bansal B. M. (1976) Chemistry, classification and petrogenesis of Apollo 17 mare basalts. *Proc. Lunar Sci. Conf. 7th.* This volume.

Sato M. (1976) Oxygen fugacity and other thermochemical parameters of Apollo 17 high-titanium basalts and their implications on the reduction mechanism. *Proc. Lunar Sci. Conf. 7th.* This volume.

Schreiber H. D. and Haskin L. A. (1976) Cr(III)–Cr(II) distribution coefficients in synthetic silicate systems in relation to the partition of chromium on the moon (abstract). In *Lunar Science VII*, p. 776–778. The Lunar Science Institute, Houston.

Usselman T. M. (1975) Ilmenite chemistry in mare basalts—an experimental study. In *Papers presented to the Conference on Origins of Mare Basalts and Their Implications for Lunar Evolution*, p. 164–168. The Lunar Science Institute, Houston.

Usselman T. M., Lofgren G. E., Donaldson C. H., and Williams R. J. (1975) Experimentally reproduced textures and mineral chemistries of high-titanium mare basalts. *Proc. Lunar Sci. Conf. 6th*, p. 997–1020.

Walker D., Kirkpatrick R. J., Longhi J., and Hays J. F. (1976a) Crystallization history and origin of lunar picritic basalt 12002: Phase equilibria and cooling rate studies. *Bull. Geol. Soc. Am.* **89**, 646–656.

Walker D., Longhi J., and Hays J. F. (1976b) Heterogeneity in titaniferous lunar basalts. *Earth Planet. Sci. Lett.* **30**, 27–36.

Wechsler B. A., Prewitt C. T., and Papike J. J. (1975) Structure and chemistry of lunar and synthetic armalcolite (abstract). In *Lunar Science VI*, p. 860–862. The Lunar Science Institute, Houston.

Williams R. J. (1971) Reaction constants in the system Fe–MgO–SiO_2–O_2 at 1 atm between 900° and 1300°C: Experimental results. *Amer. J. Sci.* **270**, 334–360.

Williams R. J. and Mullins O. (1976) A system using solid ceramic oxygen electrolyte cells to measure oxygen fugacities in gas-mixing systems. NASA Technical Memorandum, NASA TMX-58167.